



HierAttn: Effectively Learn Representations from Stage and Branch Attention for Skin Lesions Diagnosis

Wei Dai^a, Rui Liu^a, Tianyi Wu^a, Min Wang^a, Jianqin Yin^b, Jun Liu^{a,*}

^aDepartment of Mechanical Engineering, City University of Hong Kong, Hong Kong, China

^bSchool of Artificial Intelligence, Beijing University of Posts and Telecommunications, Beijing, China

arXiv:2205.04326v3 [eess.IV] 16 May 2022

ARTICLE INFO

Article history:

Received 07 May 2022

Received in final form xx xx 2022

Accepted xx xx 2022

Available online xx xx 2022

Communicated by xxx xxx

Keywords: Skin lesions classification, Same channel attention, Hierarchical pool, Stage attention, Branch attention

ABSTRACT

Accurate and unbiased examinations of skin lesions are critical for early diagnosis and treatment of skin conditions and disorders. Visual features of skin lesions vary significantly because the skin images are collected from patients with different skin colours by using dissimilar type of imaging equipment. Recent studies have reported ensembled convolutional neural networks (CNNs) to classify the images for early diagnosis of skin disorders. However, the practical use of CNNs is limited because the majority of networks are heavyweight and inadequate to use the contextual information. Although lightweight networks (e.g., MobileNetV3 and EfficientNet) were developed to save the computational cost for implementing deep neural networks on mobile devices, not sufficient representation depth restricts their performance. To address the limitations, we introduce a new light and effective neural network, namely HierAttn network. The HierAttn applies a novel strategy to balance the learning local and global features by using a multi-stage attention mechanism in a hierarchical architecture. The efficacy of HierAttn was evaluated by using the dermoscopy images dataset ISIC2019 and smartphone photos dataset PAD-UFES-20. The experimental results show that HierAttn achieves the best top-1 accuracy and AUC among the state-of-the-art light-weight networks. The new light HierAttn network has the potential in promoting the use of deep learning in clinics and allowing patients for early diagnosis of skin disorders with personal devices. The code is available at <https://github.com/anthonyweidai/HierAttn>.

© 2022 . All rights reserved.

1. Introduction

Skin conditions and disorders are among the most common human diseases to affect millions of people (Guy Jr et al., 2015a,b). Statistical data shows that around 20% of Americans are diagnosed with malignant cutaneous diseases (Esteva et al., 2017). Skin cancer, consisting of non-melanoma and melanoma, affected more than 1.5 million new cases globally in 2020 (Sung et al., 2021). It is also estimated to be the fifth

most common detected cancer in the U.S. with 196,060 new cases reported in 2021 (Fund, 2021; Sung et al., 2021). The annual cost of treating skin cancer is projected to triple from 2011 to 2030 (Guy Jr et al., 2015b). Proactive detection and early diagnosis are critically important to save patients. For instance, the five-year survival rate for melanoma could be 99% with early-stage diagnosis and treatment, whereas the survival rate is dropped to around 27% if the conditions are detected in the late stage (Fund, 2021; Sung et al., 2021).

Traditional methods for detecting skin disorders include skin cancer screening by self-examination and clinical examination. Self examination is the most common method for the

*Corresponding author.

e-mail: jun.liu@cityu.edu.hk (Jun Liu)

early detection of skin diseases. Around 53% of patients with melanomas are self-examined before approaching medical experts (Avilés-Izquierdo *et al.*, 2016). With limited professional knowledge, most patients have doubts in their examination results and feel uncertain about which type of skin disorders they have. In contrast, clinical skin examination is able to provide affirmative screening of skin cancers with a high detection accuracy (Loescher *et al.*, 2013). However, the clinical examinations consumes a considerable amount of time for medical professionals to review a large number of dermoscopic images. The long waiting time in weeks or months could delay the treatment and result in the unexpected progress of the skin conditions.

The advances of imaging technology makes it possible to diagnose skin lesions by analysing optical images of the skin lesions. The imaging modalities in skin examination include dermoscopy, reflectance confocal microscopy, total body photography, and teledermatology. Among all the imaging modalities, dermoscopy is a non-invasive imaging method without reflecting light to examine the skin lesions with up to 10x magnification (Loescher *et al.*, 2013). The review of dermoscopic images is time-consuming, and the examination results are subjective to the healthcare providers. The diagnostic accuracy requires extensive training, practice, and professional experience in understanding various features and morphologies (Rosendahl *et al.*, 2011).

Due to the sophisticated features of skin lesion images, it is nontrivial to detect skin cancer automatically with a satisfactory accuracy. Through decades of development in artificial intelligence technologies and computer hardware, deep learning has demonstrated great potentials to classify multi-class objects and outperform most experts in medical applications (Tschandl *et al.*, 2020). Well-trained deep learning models make it possible to detect skin cancer in an early, treatable stage. Recently, ensemble models such as ResNeXt, NAS-Net, SENet, DenseNet121, EfficientNet were applied in skin cancer detection and achieved the accuracy up to 94.2% and 92.6% on the ISIC2018 and ISIC2019 datasets, respectively (Adegun and Viriri, 2021). However, these ensemble models consume substantial computational resources and are highly time-consuming. Furthermore, these networks are limited in

processing the global representations of the skin lesion images. The lightweight algorithms can assist dermatologists in conducting direct skin cancer screening with limited computational resources from clinical computers. Moreover, even non-professional people, specifically the patients, have a chance to pre-distinguish symptoms of skin cancer at home by such lightweight models.

This article aims to address the challenges in balancing the reliability and accuracy for detection of skin cancers with small memory storage and minimal computational cost. The major novelty and key contributions of this study are:

- We introduce a new lightweight and low latency architecture, HierAttn [see Fig. 1], to distinguish multi-class skin lesions. The novel techniques embedded in HierAttn are the same channel attention, stage attention, and branch attention. HierAttn achieves top-level performance on the ISIC2019 and PAD-UFES-20 datasets while maintaining a small size as classic mobile deep learning models.
- We propose the same channel attention module after depth-wise convolution, which outperforms similar attention methods like squeeze and excitation.
- We use branch attention blocks based on a hierarchical pooling architecture to progressively learn both local and global representations from censorious learning stages.
- We introduce a new comprehensive data balance method and prove that it outperforms random sampling techniques for detecting skin lesions.

We review related literature in Sec. 2 and explain our proposed methodology in Sec. 3. Finally, we show the experiment results in Sec. 4, discuss the results in Sec. 5 and summarise our findings in Sec. 6.

2. Related Work

Data Processing. Three commonly used skin lesions datasets (e.g., HAM10000, ISIC2019, PAD20) are utilised in this study for the development and evaluation of deep learning models. All three datasets have the problem of large-scale data imbalance, which significantly damages the performance

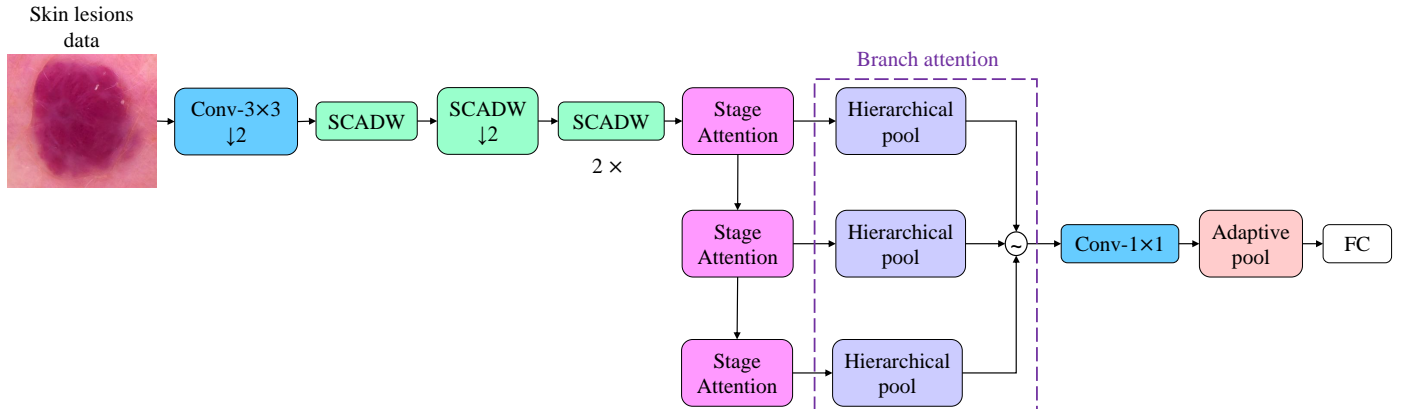


Fig. 1: **HierAttn architecture.** Conv- $n \times n$ represents a standard convolution and SCADW refers to a depth-wise separable convolution block. Down-sampling blocks are marked with $\downarrow 2$. Each stage attention has a SCADW block followed by a convolution-transformer hybrid block.

of deep learning algorithms. Possible solutions are to perform data balancing or few-shot learning (Prabhu *et al.*, 2018; Weng *et al.*, 2020). Other solutions include the modified loss function that was specifically designed to deal with the heavily imbalanced dataset (Roy *et al.*, 2022). However, the improvement of the modified loss function is relatively limited because they are more likely to misclassify the classes with a rare number of samples. Machine learning approaches are employed to analyse data such as their “hardness” and alleviate the effects of class overlap (Smith *et al.*, 2014). Due to the differences in the illumination condition and acquisition device, the colours and contrast of images are not consistent and introduce additional challenges for the classification. To deal with various imaging conditions, colour constancy algorithms were proposed by calibrating skin lesion images’ colour and the shade-of-grey method outperforms gray world, max-RGB, and general gray world methods (Barata *et al.*, 2014).

CNNs in Skin Lesions Diagnosis. The recent advances in machine learning have introduced an increasing number of deep neural networks. The deep learning models, including Inception V3, VGG, EfficientNet, ResNet, DenseNet, etc., have been applied to the classification of skin lesions (Esteva *et al.*, 2017; Weng *et al.*, 2020; Gessert *et al.*, 2020). Moreover, the models, assembling ResNeXt, NASNet, SENet, DenseNet121, and EfficientNet in several streams or stages, were utilised in skin lesions classification (Gessert *et al.*, 2020; Mahbod *et al.*, 2020; Attique Khan *et al.*, 2021). The ISIC2019 challenge winner applied an ensemble EfficientNet to achieve a 92.6% average classification accuracy; however, the model has heavy weight with more than 100 M parameters, making it impractical for clinical and home use (Gessert *et al.*, 2020). To reduce computational cost and model weight, researchers applied the depth-wise separable convolution methods. Based on such convolution method, MobileNetV2, MobileNetV3, MnasNet, and ShuffleNet were constructed and obtained relatively satisfactory performance (Sandler *et al.*, 2018; Zhang *et al.*, 2018; Tan and Le, 2019; Tan *et al.*, 2019; Howard *et al.*, 2019). However, the performance of these light networks remains unknown for the skin lesion analysis.

Attention Mechanisms. The attention mechanism is a biomimetic cognitive method used in diverse computer vision assignments such as image classification (Woo *et al.*, 2018; Hu *et al.*, 2018; Dosovitskiy *et al.*, 2020; Hou *et al.*, 2021; Mehta and Rastegari, 2021) and image segmentation (Mehta and Rastegari, 2021; He *et al.*, 2022). An example of the attention network is the SENet, which obtains global representations by average global pooling and channel-wise feature response by squeeze and excitation (Hu *et al.*, 2018). The convolution block attention module (CBAM) improves the SENet by using a larger kernel size to encode spatial information (Woo *et al.*, 2018). Coordinated attention further advances the average global pooling by encoding channel relationships and long-range dependencies via average pooling along different axes (Hou *et al.*, 2021). However, they introduce more learnable parameters and consume more computational resources than previous methods.

To improve the computational efficiency and meet the scal-

ability requirement, self-attention mechanisms, particularly transformers, are introduced into computer vision from natural language processing. With self-attention, a vision transformer (ViT) replaces the traditional convolution method with a transformer encoder (Dosovitskiy *et al.*, 2020). Because the input images are directly split into patches and embedded, the ViT models are still quite large, with more than 100 M parameters (Dosovitskiy *et al.*, 2020). To reduce the latency of splitting images, computer scientists from Apple proposed MobileViT by applying the MobileNet V2 block to compose images and then used a transformer to process the information (Mehta and Rastegari, 2021). MobileViT has been reported as an effective network for image classification while maintaining a lightweight.

3. Proposed Methodology

3.1. Skin Lesion Dataset

ISIC2019 (Tschandl *et al.*, 2018; Adegun and Viriri, 2021; Combalia *et al.*, 2019) and PAD-UFES-20 (PAD20) (Pacheco *et al.*, 2020), two publicly available skin lesions datasets, are used in this research for development and evaluation of the proposed methods. ISIC2019 dataset consists of 25,331 dermoscopy images with eight categories: actinic keratosis (ACK), basal cell carcinoma (BCC), benign keratosis (BKL), dermatofibroma (DF), melanoma (MEL), melanocytic nevus (NV), squamous cell carcinoma (SCC), vascular lesion (VASC) (Tschandl *et al.*, 2018; Adegun and Viriri, 2021; Combalia *et al.*, 2019). Three of them belong to the non-melanoma skin cancer, ACK, BCC and SCC. Melanoma is the most sever skin cancer that is caused by the uncontrolled growing cells that can produce pigment. The vascular lesions (VASC) can be either benign or malignant and requires close monitoring over a period of time. The remaining categories of skin lesions are benign conditions.

The PAD20 dataset includes 2,298 skin lesion images collected by using smartphones. The PAD20 dataset has six classes: ACK, BCC, BKL, MEL, NV, and SCC (Pacheco *et al.*, 2020). Compared to ISIC2019, PAD20 has two fewer classes, DF and VASC, because of lacking photos of skin lesions. The data distribution of the two datasets is shown in Fig. 2. Dermoscopy and smartphones are two standard methods to capture skin lesions images. Thus, the two datasets effectively represent current image data for classification of skin lesions.

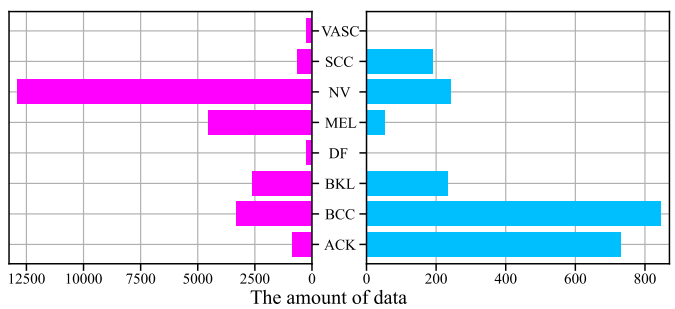


Fig. 2: **Data distribution** on ISIC2019 (left image) and PAD20 (right image)

3.2. Pre-processing

3.2.1. Image pre-processing

The data among different classes from the ISIC2019 dataset has large black area [see Fig. 3 (a)], which damage the evaluation performance of models. Thus, an adaptive cropping method is taken to identify and crop these images. The original image is first turned into greyscale [Fig. 3 (b)] and then binarized an adaptive threshold ranging from 50 to 255 [Fig. 3 (c)]. After that, the contour of the binarized image is detected to confirm the circle location. When the value of the circle area divided by the whole image area is between 0.01 and 0.9, the region enclosed by the circle is cropped and saved [Fig. 3 (d)]. Post-processing inspection by multiple users indicates that the method is robust.

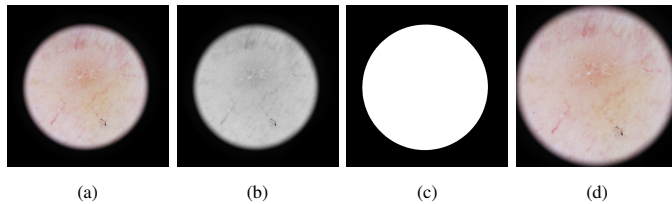


Fig. 3: **The progress in cropping image** (a) original image, (b) greyscaled image, (c) binarized image, and (d) cropped image.

3.2.2. Data balance

In this study, an imbalance ratio is defined to quantitatively assess the imbalance problem. The imbalance ratio is the ratio of images of the majority class over the minority class. The imbalance ratio for ISIC2019 and PAD20 are 53.9 and 16.3, respectively. Such imbalance ratios can remarkably reduce the performance of deep learning, according to previous research (Buda et al., 2018). The data imbalance could lead to a low validation result on the minority class, though the averaged validation metrics over all classes could be high. Data balance by oversampling or undersampling for each class is a practical technique to handle the dataset with a large imbalance ratio. Oversampling and undersampling are simultaneously utilised to balance ISIC2019 and PAD20 data. After sampling, 2500 images and 500 images are collected for each class in the ISIC2019 and PAD20 datasets, respectively. Thus, the amount of data after balancing totals 20000 and 3000 on ISIC2019 and PAD20, respectively, close to the total amount of unbalanced data.

Oversampling uses horizontal flips, random crops, Gaussian blur, linear contrast, random translation, rotation, and shear on a small scale to generate new images from the old images. As for undersampling, the random selection of a fixed number of images tend to have a class-overlapping problem. Thus, we propose an adaptive data analysis method called instance hardness (IH) to alleviate this adverse effect. Instance hardness can be defined as (Smith et al., 2014):

$$IH_{\mathcal{L}}(\langle x_i, y_i \rangle) = 1 - \frac{1}{|\mathcal{L}|} \sum_{j=1}^{|\mathcal{L}|} p(y_i|x_i, g_j(t, \alpha)) \quad (1)$$

where \mathcal{L} is a prior with non-zero probability while treating all other learning algorithms as having zero probability, g is a ma-

ching learning algorithm trained on t with hyper-parameters α , and y_i is the label for data x_i .

Outliers and mislabelled data are expected to have high IH. Thus, IH analysis was applied in undersampling to remove those data with a high IH. This research uses the random forest as the machine learning method g , referenced from the imbalanced-learn study (Lemaître et al., 2017). Datasets after sampling are renamed as IHISIC20000, RandISIC20000, IH-PAD3000 and RandPAD3000. Randomly oversampling is applied to these four datasets. IH and Rand represent the dataset using instance hardness and random sampling methods for undersampling, respectively. Moreover, 20000 and 3000 are the total number of images in the datasets.

3.3. HierAttn Architecture

The standard transformer has been applied to process sequences of image patches to learn the inter-patch representations. However, this type of transformer method ignores the inductive biases (e.g., translation equivariance and locality) inherent to CNNs, which leads to poor performance while training with insufficient data (Dosovitskiy et al., 2020). MobileViT is a transformer-based method proposed to tackle the loss of inductive biases by taking convolution and transformer to form a hybrid block (Mehta and Rastegari, 2021). However, it can not thoroughly learn representation due to the information lost. Multilevel loss is widely used to extract feature information from stages to improve the model's performance. For instance, GoogleNet has three losses and adds them together to form the total loss in training (Szegedy et al., 2015). However, the features in various stages are directly fed into simple tensor operations. They do not have any correlation influence on each other.

The paper introduces an efficient and lite Convolution-Transformer model [see Fig. 1]. The main idea of this model is to learn the local and global representations by utilising attention and self-attention mechanisms simultaneously. The hierarchical branches allow the network to keep various information from different depths of layers.

3.3.1. Same Channel Attention

The block modifies the depth-wise separable convolution (DWSConv) with the same channel attention (SCAttn) technique and result in a new block structure called SCADW block (i.e., green blocks in Fig. 1). Fully convolution has a high computation cost. Google researchers utilised the DWSConv block to reduce the model size (Sandler et al., 2018). Squeeze and excitation attention (SEAttn) blocks were proposed to enhance the expressive power of the learned features after depth-wise convolution in the MobileNetV3 block (Howard et al., 2019). However, the point-wise convolution already extracts the channel-wise information, which suggests that the excitation of SEAttn is more likely a redundant operation. Therefore, the SCAttn is introduced in this study after depth-wise convolution by utilising the attention mechanisms while maintaining the same number of learnable parameters as the DWSConv block. The SCAttn block is illustrated in Fig. 4.

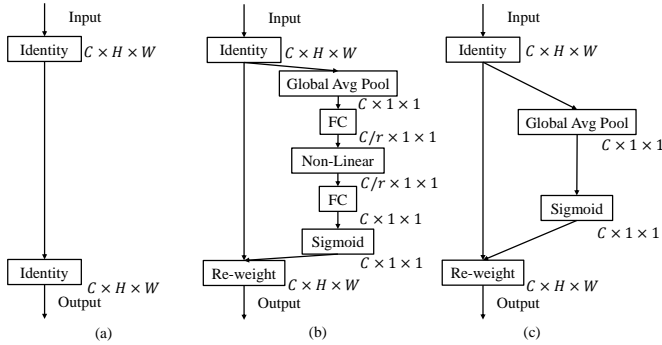


Fig. 4: Schematic comparison of the original block (without attention mechanism) (a), the SEAttn block (b), and the proposed SCAttn block (c).

3.3.2. Stage attention

Each stage attention module (i.e., pink blocks in Fig. 1) has a SCADW block with a stride of 2 followed by a convolution-transformer hybrid block. Inspired by the MobileViT architecture (Mehta and Rastegari, 2021), we simultaneously apply the convolutions and transformers to learn the local and global representations of an input skin lesion image with fewer parameters. The convolution-transformer hybrid (CTH) block steadily conducts unfolding, transformer encoding and folding like standard convolutions (Mehta and Rastegari, 2021). Thus, the CTH block has inductive bias and can process the transformers with convolutions. Recently, vision transformers (ViTs) utilising multi-head self-attention mechanisms have shown great potential in classification tasks (Dosovitskiy et al., 2020). The CTH block also consists of a multi-head self-attention followed by a multilayer perceptron (MLP) layer. Furthermore, we also add a skip connection to link the input and output of the CTH block.

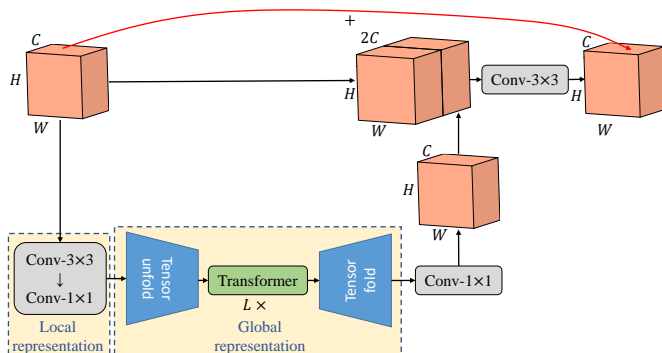


Fig. 5: Convolution-transformer hybrid block.

3.3.3. Branch attention

In this study, we propose to use hierarchical pooling and tensor assembling to downsize tensors and learn features from different stages simultaneously. This new technique aims to utilise and improve the interactions of features among different learning stages. Moreover, by keeping the different sizes of pooling results, hierarchical pooling learns the local representation of tensors with large tensor size ($C \times 5 \times 5$) and attains tensors' global representation with small tensor size ($C \times 1 \times 1$). Moreover, the medium tensor size ($C \times 3 \times 3$) is also designed as a

buffer layer to keep both local and global features. The pooled tensors from different branches are then channel-wisely assembled. After that, channel-wise ensembled tensors are pixel-wisely assembled. At the end of branch attention, the pixels of assembled tensors are pixel-wisely randomised by utilising the Monte Carlo method. The branch attention progress is illustrated in Fig. 6. Stage attention thoroughly rearranges feature maps by downsizing feature maps, and the processed features are further extracted by the CTH block as described in the aforementioned section. The branch attention is applied as a particular learning stage after each stage attention block.

3.3.4. Small-scale transformer

Learning global information by transformers utilises fewer parameters than convolutions. However, transformer operations lose spatial bias, increasing computational costs to learn visual representations (Mehta and Rastegari, 2021). Thus, they are wide and deep. ViT-Base, ViT-Large, and ViT-Huge models use the number of transformer blocks $L=12, 24, 32$ and the number of embedded dimensions $d = 768, 1024, 1280$, respectively (Dosovitskiy et al., 2020). However, our new HierAttn only requires $L = 2, 4, 3$ and $d = 96, 120, 144$, are reference from MobileViT architecture. The number of parameters for the new HierAttn and other state-of-the-art networks is summarised in Table 1.

3.3.5. HierAttn architecture

The full name of HierAttn is hierarchical attention. On the one hand, we use SCADW in each stage attention to process low-level to high-level features. On the other hand, we use hierarchical pooling to obtain hierarchical sizes of tensors, $C \times 5 \times 5$, $C \times 3 \times 3$ and $C \times 1 \times 1$, for learning local and global representations at different degrees. HierAttn is inspired by the philosophy of making full use of local and global information on the tensors and stage conditions of the network. We train HierAttn models at two different network sizes (S: small, XS: extra small). The SCADW blocks in HierAttn are typically responsible for decreasing tensors' size while alleviating the information loss. The initial layer of stage attention is a 3×3 standard convolution with a stride of 2, following SCADW blocks and stage attention modules. Moreover, all stage representations are further handled by the branch attention. Furthermore, stochastic depth is applied on every SCADW block and CTH block with a stride of 1 to reduce time cost and validation error.

4. Experimental Results

In this section, we first evaluate HierAttn performance on the IHISIC20000 and IHPAD3000 datasets in subsection 4.1. Table 1 and Fig. 7 show that HierAttn delivers significantly better performance than state-of-the-art networks. In subsection 4.2, we conducted ablation studies for data balance methods and HierAttn architecture.

4.1. Image classification on the skin lesions dataset

4.1.1. Implementation details

The HierAttn networks are trained and validated for 500 epochs on one RTX A4000 with a batch size of 64 images

using AdamW optimiser (Loshchilov and Hutter, 2017) with 10-fold cross-validation and cross-entropy loss. The learning rate is ceased from 0.002 to 0.0002 during the first 15 epochs and then increased to 0.0002 utilising the cosine scheduler (Loshchilov and Hutter, 2016). L2 weight decay of 0.01 is adopted. Knowledge transfer is applied to reduce the training time and improve model performance. The tunable parameters for initialisation of HierAttn are partly taken from MobileViT, including standard convolution, SCADW blocks, and CTH blocks. All transferred models for training in IHISIC20000 and IHPAD3000 were trained in ImageNet1k (Mehta and Rastegari, 2021; Paszke *et al.*, 2019) and IHISIC20000, respectively. Thus, the weight of the classifier is ignored while transferring weight to train our models on the skin lesions dataset. Moreover, the transfer learning warm-up is applied to alleviate the negative influence of untransferred layers on transferred layers. On the first training 30 epochs, all transferred layers are frozen. After that, gradient calculation is required for all layers with learnable parameters. In addition, the inference time for each image is calculated by averaging 1000 iterations to demonstrate HierAttn for mobile applications with slower processors.

4.1.2. Top-1 Accuracy and Inference Time

Each model with six on IHISIC20000 or eight classes on IHPAD3000 has a similar number of parameters when two decimal places are kept. Thus, the number of parameters of each model is computed with eight classes to simplify the discussion. Fig. 7 compares HierAttn with six other lightweight networks that are also trained on IHISIC20000 and IHPAD3000 datasets. Detailed values are illustrated in Table 1. Fig. 7 demonstrates that HierAttn networks fall in the upper left region, which means they outperform other mobile models with relatively small sizes. For instance, with about 1.08 million parameters, HierAttn_s outperforms MobileNetV2 by 3.25%, MobileNetV3_large by 1.93%, ShuffleNetV2_1x by 1.47%, MnasNet1.0 by 1.25%, and EfficientNet-b0 by 0.55% on IHISIC20000 validation set. Furthermore, HierAttn_s also outperforms MobileViT_s, which is also a convolution-transformer hybrid model, by 1.98% and 3.00% on IHISIC20000 and IHPAD3000 datasets, respectively. Moreover, Table 1 shows the

inference time for each image by different models. The inference time for each image by HierAttn_xs is lower than 1 ms, 12% faster than MnasNet1.0's and just 9% slower than MobileNetV2's.

4.1.3. ROC and AUC

In this paper, the receiver operating characteristic (ROC) curve and its area under the curve (AUC) are applied to demonstrate the general performance of each model. The results can be found in Fig. 8. The figure represents that all models on experiments have more than 0.99 AUC on the IHISIC20000 and 0.98 AUC on the IHPAD3000 validation set, suggesting that they possess satisfactory analytical capacities to conduct multi-classes lesions classification tasks. Furthermore, the ROCs of HierAttn_s and HierAttn_xs are the first and second closest to the point (0, 1) on both IHISIC20000 and IHPAD3000 validation sets. Moreover, HierAttn_s and HierAttn_xs have the first and the second largest AUC on both datasets among all models, for instance, 0.99772 and 0.99558 on the IHISIC20000 validation set, respectively. Thus, the ROCs and AUCs show that HierAttn is the most reliable and superlative model to detect skin lesions among current conventional and advanced mobile models. Meanwhile, the same model's AUC of the IHPAD3000 validation set is lower than the IHISIC20000 validation set, which means these models perform better on the IHISIC20000 validation set.

In conclusion, these experimental results prove that HierAttn is robust and effective. Thus, it can be practically applied to skin lesions diagnosis.

4.2. Ablation studies

4.2.1. Implementation details

In ablation studies, the model used is HierAttn_s, and the dataset used is IHISIC20000, if not mentioned. Other parameters are the same as Section 4.1.

4.2.2. Data balance methods

Fig. 9 illustrates the top-1 accuracy of different data balance methods on ISIC20000 and PAD3000. Firstly, the top-1 accu-

Table 1: # Parameters, inference time, and top-1 accuracy of different models.

Model	# Parameters/M	Inference time/ms	Top-1 Accuracy/%	
			IHISIC20000 \uparrow	IHPAD3000
MobileNetV2 (Sandler <i>et al.</i> , 2018)	2.23	0.802	93.45	87.44
MobileViT_s (Mehta and Rastegari, 2021)	4.94	1.528	94.72	88.22
MobileNetV3_Large (Howard <i>et al.</i> , 2019)	4.21	0.538	94.77	88.78
ShuffleNetV2_1x (Zhang <i>et al.</i> , 2018)	2.28	0.307	95.23	87.89
MnasNet1.0 (Tan <i>et al.</i> , 2019)	3.11	0.997	95.45	90.33
EfficientNet_b0 (Tan and Le, 2019)	4.02	0.586	95.48	90.22
HierAttn_xs (ours)	1.08	0.878	96.15	90.11
HierAttn_s (ours)	2.14	1.658	96.70	91.22

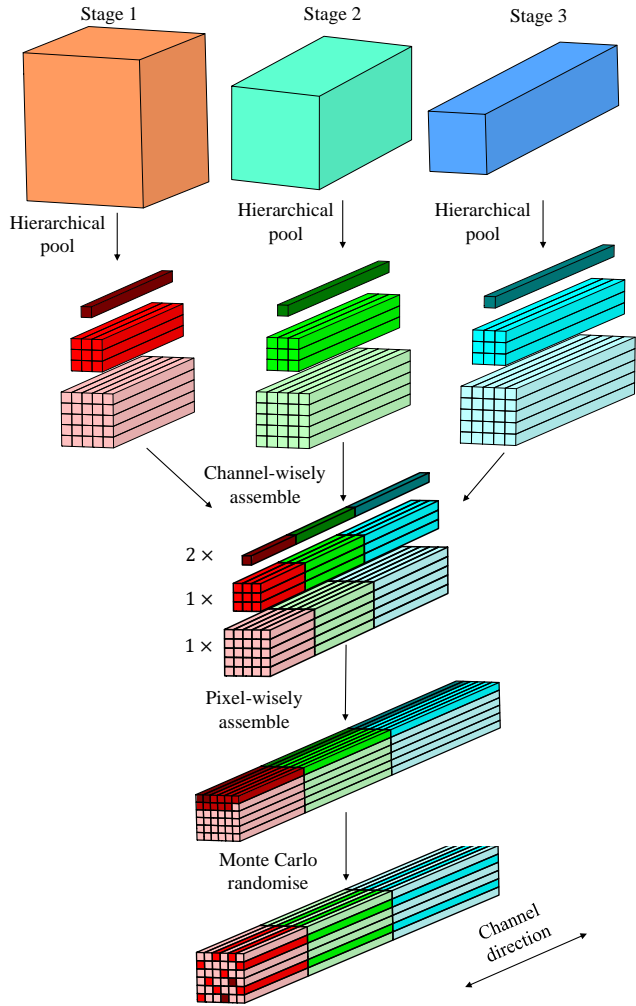


Fig. 6: Branch attention by hierarchical pooling, assembling branch tensors and randomising tensors.

racy of IH (instance hardness) is higher than that of Rand (randomised sampling) on both datasets, which means IH can more effectively sample images than Rand. Secondly, IH exceeds 5.9% and 0.7% top-1 accuracy than Rand in ISIC20000 and PAD3000, respectively. The diminishing improvement on the PAD dataset could be caused by the low imbalance ratio of PAD compared to the ISIC dataset (16.3 for PAD vs. 53.9 for ISIC). The effects of alleviating negative influence on classification are more obvious for the dataset with a high imbalance ratio. Thirdly, the error bar of ISIC20000 is shorter than PAD3000, indicating that HierAttn is more robust on ISIC20000 than PAD3000.

4.2.3. Attention blocks in DWSConv

Table 2 shows the number of parameters, inference time and top-1 accuracy of models using different attention mechanisms in DWSConv. It can be discovered that without the attention mechanism [see Fig. 4 (a)], the network only achieved only 96.20% top-1 accuracy. However, HierAttn with SEAttn or SCAttn attains at least 4.5% more top-1 accuracy than without using the attention mechanism in DWSConv. Although the top-1 accuracy of HierAttn with SCAttn is only 0.5% more than

HierAttn with SEAttn, HierAttn with SCAttn is faster for inference with smaller the number of parameters than HierAttn with SEAttn.

Table 2: Properties of different attention mechanisms in DWSConv.

Attention mechanism	# Parameters/M	Inference time/ms	Top-1 Accuracy/%
-	2.14	1.551	96.20
SEAttn	2.17	1.663	96.65
SCAttn	2.14	1.658	96.70

5. Discussion

From Table 2, we can discover that even without attention after depth-wise convolution, HierAttn still achieves the most considerable top-1 accuracy, 96.20%, on the IHISIC20000 validation set. It suggests that branch attention could be preferable to obtaining critical stages' information. It also shows a high potential to use branch attention as a general method for improving the performance of different models. Applying branch attention in a model with more layers, e.g., 300, can prevent the gradient descent in back-propagation. Although branch attention needs additionally computational resources, we can still carefully select typical stages to apply branch attention.

Due to the limited computation resources, the transferred weight of HierAttn is partly from MobileViT. Thus, branch attention and classifier in HierAttn do not have transferred weight. It is suggested that HierAttn could have more excellent performance if we could fully pre-train the network on the ImageNet1k dataset.

We also discover that the model pre-trained in dermatoscopy dataset IHISIC20000 has around 6% more accuracy while training in smartphone dataset IHPAD3000 than the model pre-trained in ImageNet1k. The result suggests that the prediction accuracy could be increased if we have a larger smartphone dataset for pre-training our models.

We also proposed a larger version of HierAttn, HierAttn_m, with 5.44 M parameters. However, we have not trained or validated HierAttn_m yet due to limited computation resources. We believe it also has appreciable potential to detect skin lesions in large hospitals or clinical centres than can support heavy computing in routine examinations.

Mobile application for skin cancer diagnosis allows dermatologists to perform point of care testing. Moreover, possible patients can carry out further detection by utilising mobile applications while doing regular self-exam. HierAttn has a statistically close speed to classic mobile networks, which shows great potential to be developed on mobile devices. If the skin lesion is recognised as MEL, BCC, ACK, SCC and VASC with more than 50% possibility, users are suggested to go to a clinic or hospital to perform further diagnosis. Otherwise, it is more likely that the detected area of the skin is healthy. We expect that HierAttn can be deployed on the mobile phone to assist ordinary people in performing regular self-check in the future.

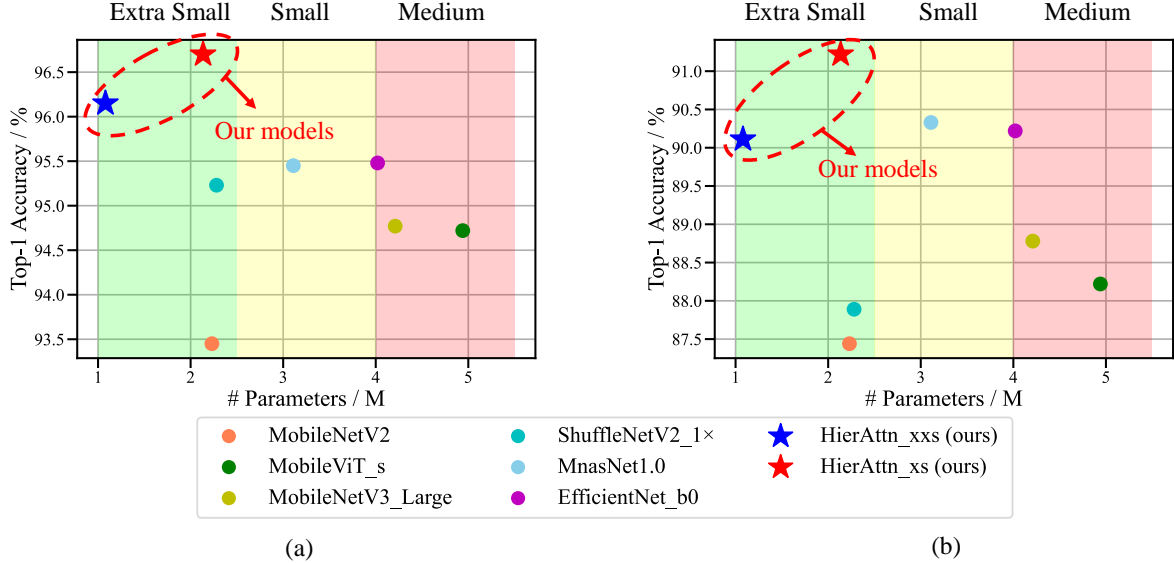


Fig. 7: HierAttn vs. classic mobile models on (a) IHISIC20000 and (b) IHPAD3000 validation set.

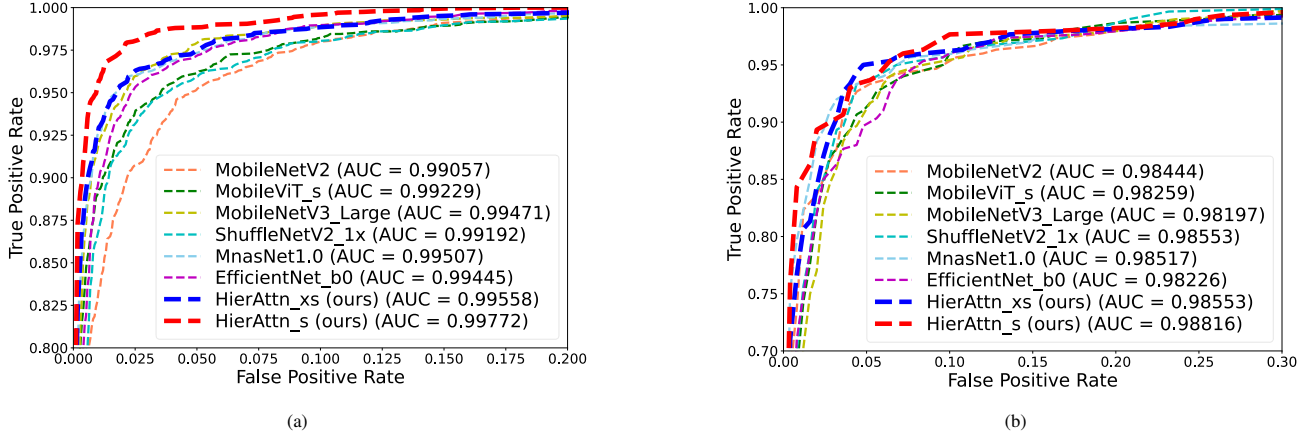


Fig. 8: ROC curves of different classification methods on skin lesions dataset (a) IHISIC20000 validation set and (b) IHPAD3000 validation set.

6. Conclusion

In this paper, we propose a HierAttn network consisting of SCAttn, stage attention, and branch attention for skin lesions diagnosis. SCAttn directly extracts global features by only global average pooling without operating channel-wise information abundantly. Stage attention consists of a SCADW block to downsize feature maps and a CTH block to learn local and global representations effectively. Branch attention applies hierarchical pooling after each stage attention to learn local and global representations while improving the interaction of feature relationships. Additionally, we propose a comprehensive data balance method based on instance hardness analysis undersampling and random oversampling. With these novel modules, HierAttn can achieve better skin lesions classification results, 96.70% top-1 accuracy and 0.9972 AUC on IHISIC20000 and 91.22% top-1 accuracy and 0.98816 AUC on IHPAD3000 validation set, than other state-of-the-art mobile networks.

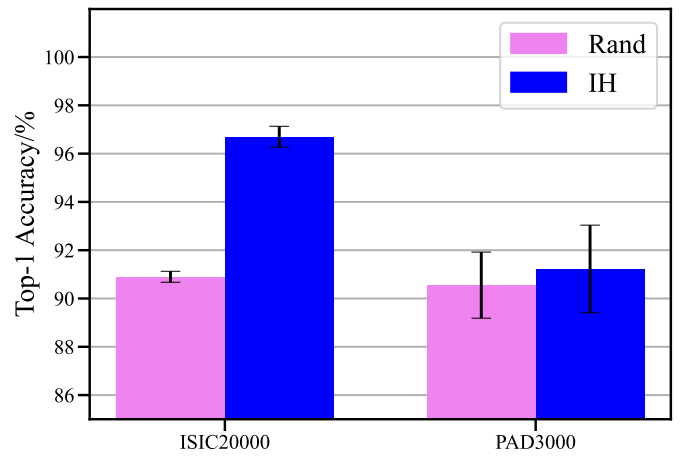


Fig. 9: Top-1 Accuracy of different data balance methods.

Acknowledgments

This work was supported by the Research Grant Council (RGC) of Hong Kong under Grant 11212321 and Grant ECS-

21212720, Guangdong Province Basic and Applied Basic Research Fund Project 2019A1515110175, and Science and Technology Innovation Committee of Shenzhen under Grant Type-C 2022/86.

References

Adegun, A., Viriri, S., 2021. Deep learning techniques for skin lesion analysis and melanoma cancer detection: a survey of state-of-the-art. *Artificial Intelligence Review* 54, 811–841.

Attique Khan, M., Sharif, M., Akram, T., Kadry, S., Hsu, C., 2021. A two-stream deep neural network-based intelligent system for complex skin cancer types classification. *International Journal of Intelligent Systems* .

Avilés-Izquierdo, J.A., Molina-López, I., Rodríguez-Lomba, E., Marquez-Rodas, I., Suarez-Fernandez, R., Lazaro-Ochaita, P., 2016. Who detects melanoma? impact of detection patterns on characteristics and prognosis of patients with melanoma. *Journal of the American Academy of Dermatology* 75, 967–974.

Barata, C., Marques, J.S., Celebi, M.E., 2014. Improving dermoscopy image analysis using color constancy, in: 2014 IEEE International Conference on Image Processing (ICIP), IEEE. pp. 3527–3531.

Buda, M., Maki, A., Mazurowski, M.A., 2018. A systematic study of the class imbalance problem in convolutional neural networks. *Neural Networks* 106, 249–259.

Combalia, M., Codella, N.C., Rotemberg, V., Helba, B., Vilaplana, V., Reiter, O., Carrera, C., Barreiro, A., Halpern, A.C., Puig, S., et al., 2019. Bcn20000: Dermoscopic lesions in the wild. *arXiv preprint arXiv:1908.02288* .

Dosovitskiy, A., Beyer, L., Kolesnikov, A., Weissenborn, D., Zhai, X., Unterthiner, T., Dehghani, M., Minderer, M., Heigold, G., Gelly, S., et al., 2020. An image is worth 16x16 words: Transformers for image recognition at scale. *arXiv preprint arXiv:2010.11929* .

Esteva, A., Kuprel, B., Novoa, R.A., Ko, J., Swetter, S.M., Blau, H.M., Thrun, S., 2017. Dermatologist-level classification of skin cancer with deep neural networks. *nature* 542, 115–118.

Fund, W.C.R., 2021. Cancer facts and figures 2021. I2.

Gessert, N., Nielsen, M., Shaikh, M., Werner, R., Schlaefter, A., 2020. Skin lesion classification using ensembles of multi-resolution efficientnets with meta data. *MethodsX* 7, 100864.

Guy Jr, G.P., Machlin, S.R., Ekwueme, D.U., Yabroff, K.R., 2015a. Prevalence and costs of skin cancer treatment in the us, 2002–2006 and 2007–2011. *American journal of preventive medicine* 48, 183–187.

Guy Jr, G.P., Thomas, C.C., Thompson, T., Watson, M., Massetti, G.M., Richardson, L.C., 2015b. Vital signs: melanoma incidence and mortality trends and projections—united states, 1982–2030. *MMWR. Morbidity and mortality weekly report* 64, 591.

He, X., Tan, E.L., Bi, H., Zhang, X., Zhao, S., Lei, B., 2022. Fully transformer network for skin lesion analysis. *Medical Image Analysis* , 102357.

Hou, Q., Zhou, D., Feng, J., 2021. Coordinate attention for efficient mobile network design, in: Proceedings of the IEEE/CVF Conference on Computer Vision and Pattern Recognition, pp. 13713–13722.

Howard, A., Sandler, M., Chu, G., Chen, L.C., Chen, B., Tan, M., Wang, W., Zhu, Y., Pang, R., Vasudevan, V., et al., 2019. Searching for mobilenetv3, in: Proceedings of the IEEE/CVF International Conference on Computer Vision, pp. 1314–1324.

Hu, J., Shen, L., Sun, G., 2018. Squeeze-and-excitation networks, in: Proceedings of the IEEE conference on computer vision and pattern recognition, pp. 7132–7141.

Lemaître, G., Nogueira, F., Aridas, C.K., 2017. Imbalanced-learn: A python toolbox to tackle the curse of imbalanced datasets in machine learning. *The Journal of Machine Learning Research* 18, 559–563.

Loescher, L.J., Janda, M., Soyer, H.P., Shea, K., Curiel-Lewandrowski, C., 2013. Advances in skin cancer early detection and diagnosis, in: *Seminars in oncology nursing*, Elsevier. pp. 170–181.

Loshchilov, I., Hutter, F., 2016. Sgdr: Stochastic gradient descent with warm restarts. *arXiv preprint arXiv:1608.03983* .

Loshchilov, I., Hutter, F., 2017. Decoupled weight decay regularization. *arXiv preprint arXiv:1711.05101* .

Mahbod, A., Schaefer, G., Wang, C., Dorffner, G., Ecker, R., Ellinger, I., 2020. Transfer learning using a multi-scale and multi-network ensemble for skin lesion classification. *Computer Methods and Programs in Biomedicine* 193, 105475.

Mehta, S., Rastegari, M., 2021. Mobilevit: light-weight, general-purpose, and mobile-friendly vision transformer. *arXiv preprint arXiv:2110.02178* .

Pacheco, A.G., Lima, G.R., Salomão, A.S., Krohling, B., Biral, I.P., de Angelo, G.G., Alves Jr, F.C., Esgario, J.G., Simora, A.C., Castro, P.B., et al., 2020. Pad-ufes-20: a skin lesion dataset composed of patient data and clinical images collected from smartphones. *Data in brief* 32, 106221.

Paszke, A., Gross, S., Massa, F., Lerer, A., Bradbury, J., Chanan, G., Killeen, T., Lin, Z., Gimelshein, N., Antiga, L., et al., 2019. Pytorch: An imperative style, high-performance deep learning library. *Advances in neural information processing systems* 32.

Prabhu, V., Kannan, A., Ravuri, M., Chablani, M., Sontag, D., Amatriain, X., 2018. Prototypical clustering networks for dermatological disease diagnosis. *arXiv preprint arXiv:1811.03066* .

Rosendahl, C., Tschandl, P., Cameron, A., Kittler, H., 2011. Diagnostic accuracy of dermatoscopy for melanocytic and nonmelanocytic pigmented lesions. *Journal of the American academy of dermatology* 64, 1068–1073.

Roy, A.G., Ren, J., Azizi, S., Loh, A., Natarajan, V., Mustafa, B., Pawlowski, N., Freyberg, J., Liu, Y., Beaver, Z., et al., 2022. Does your dermatology classifier know what it doesn't know? detecting the long-tail of unseen conditions. *Medical Image Analysis* 75, 102274.

Sandler, M., Howard, A., Zhu, M., Zhmoginov, A., Chen, L.C., 2018. Mobiilenetv2: Inverted residuals and linear bottlenecks, in: Proceedings of the IEEE conference on computer vision and pattern recognition, pp. 4510–4520.

Smith, M.R., Martinez, T., Giraud-Carrier, C., 2014. An instance level analysis of data complexity. *Machine learning* 95, 225–256.

Sung, H., Ferlay, J., Siegel, R.L., Laversanne, M., Soerjomataram, I., Jemal, A., Bray, F., 2021. Global cancer statistics 2020: Globocan estimates of incidence and mortality worldwide for 36 cancers in 185 countries. *CA: a cancer journal for clinicians* 71, 209–249.

Szegedy, C., Liu, W., Jia, Y., Sermanet, P., Reed, S., Anguelov, D., Erhan, D., Vanhoucke, V., Rabinovich, A., 2015. Going deeper with convolutions, in: Proceedings of the IEEE conference on computer vision and pattern recognition, pp. 1–9.

Tan, M., Chen, B., Pang, R., Vasudevan, V., Sandler, M., Howard, A., Le, Q.V., 2019. Mnasnet: Platform-aware neural architecture search for mobile, in: Proceedings of the IEEE/CVF Conference on Computer Vision and Pattern Recognition, pp. 2820–2828.

Tan, M., Le, Q., 2019. Efficientnet: Rethinking model scaling for convolutional neural networks, in: International conference on machine learning, PMLR. pp. 6105–6114.

Tschandl, P., Rinner, C., Apalla, Z., Argenziano, G., Codella, N., Halpern, A., Janda, M., Lallas, A., Longo, C., Malvehy, J., et al., 2020. Human–computer collaboration for skin cancer recognition. *Nature Medicine* 26, 1229–1234.

Tschandl, P., Rosendahl, C., Kittler, H., 2018. The ham10000 dataset, a large collection of multi-source dermatoscopic images of common pigmented skin lesions. *Scientific data* 5, 1–9.

Weng, W.H., Deaton, J., Natarajan, V., Elsayed, G.F., Liu, Y., 2020. Addressing the real-world class imbalance problem in dermatology, in: *Machine Learning for Health*, PMLR. pp. 415–429.

Woo, S., Park, J., Lee, J.Y., Kweon, I.S., 2018. Cbam: Convolutional block attention module, in: Proceedings of the European conference on computer vision (ECCV), pp. 3–19.

Zhang, X., Zhou, X., Lin, M., Sun, J., 2018. Shufflenet: An extremely efficient convolutional neural network for mobile devices, in: Proceedings of the IEEE conference on computer vision and pattern recognition, pp. 6848–6856.

Supplementary Material

HierAttn architecture

The HierAttn architecture is motivated by MobileNetV3, EfficientNet, MobileViT, and GoogleNet. The first layer of the HierAttn is a standard 3×3 convolution. Learning from MobileNetV3, we employ SCADW blocks to extract features with depth-wise separable convolution and attention mechanisms followed by three-stage attentions. Referencing MobileViT, we utilise the CTH block in stage attention to learn local and global representations and Swish as the activation function (Mehta and Rastegari, 2021). EfficientNet shows insights on using stochastic depth to stabilise the training process (Tan and Le, 2019). We adopt this method in every skip connection of the HierAttn. Finally, GoogleNet has a perception that uses stage information by multi-loss during training (Szegedy *et al.*, 2015). Based on this, we further combine stage information by hierarchical pooling using hierarchical attention mechanisms. The architecture parameters are shown in Table 3.

Pre-processing

The source code for skin lesion image pre-processing like Fig. 2 is publicly available on https://github.com/anthonyweidai/circle_extractor.

Oversampling. One of the oversampling results is illustrated in Fig. 10.

IH analysis. The demonstration of IH analysis and random undersampling methods can be found in Fig. 11. The four colours represent the four undersampled classes in ISIC2019. This figure shows that IH analysis can efficiently remove outliers from the datasets, while the random undersampling method cannot, and there is a more considerable amount of overlap sampled data. Fig. 9 depicts that the performance of the HierAttn_s improves by 5.9% by using IH on ISIC20000.

Table 3: **HierAttn architecture.** Here, d means dimensionality of the input to the transformer layer in the CTH block. In the CTH block, kernel size is set as three and patch height and width are set as two.

Layer	Output size	Repeat	Output Channels	
			XS	S
Image	256×256			
Conv 3×3 , $\downarrow 2$	128×128	1	16	16
SCADW		1	16	32
Conv 3×3 , $\downarrow 2$	64×64	1	24	48
SCADW		2	24	48
Stage1	Conv 3×3 , $\downarrow 2$	1	48	64
	CTH block	1	48($d = 64$)	64($d = 96$)
Stage1	Conv 3×3 , $\downarrow 2$	1	64	80
	CTH block	1	64($d = 80$)	80($d = 120$)
Stage1	Conv 3×3 , $\downarrow 2$	1	80	96
	CTH block	1	80($d = 96$)	96($d = 144$)
Branch attention	8×8	1	192	240
Conv 1×1		1	768	960
Branch attention	1×1	1	8 or 6	8 or 6
Linear				
# Parameters			1.08 M	2.14 M

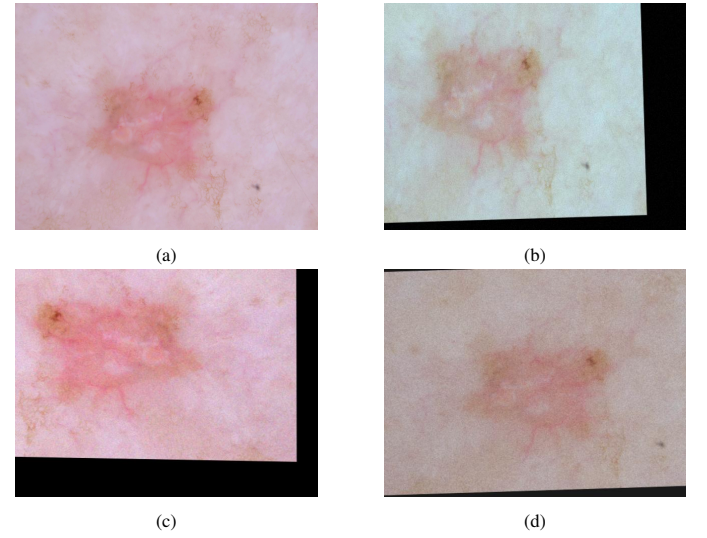


Fig. 10: **Schematic illustration of oversampling results** (b)(c)(d) and original image ISIC_0024946.jpg (a).

Additional ablations

Transfer learning warm-up. We consider that the models are unstable after partially transferring tunable parameters, and statistical methods randomly initialise those layers without transferring. We apply a warm-up technique to alleviate the influence of random weight initialisation for transferred layers. We freeze the transferred layers, locking gradient descent, in the first 30 epochs. In these 30 epochs, only those layers without transferring can update their parameters. Table 4 shows that the performance of the HierAttn_s improves by 0.42% on the IHISIC2019 dataset.

Stochastic depth. Stochastic depth, also regarded as “layer dropout”, is implemented in each layer with a skip connection in HierAttn. Typically, it is in all SCADW blocks with a stride

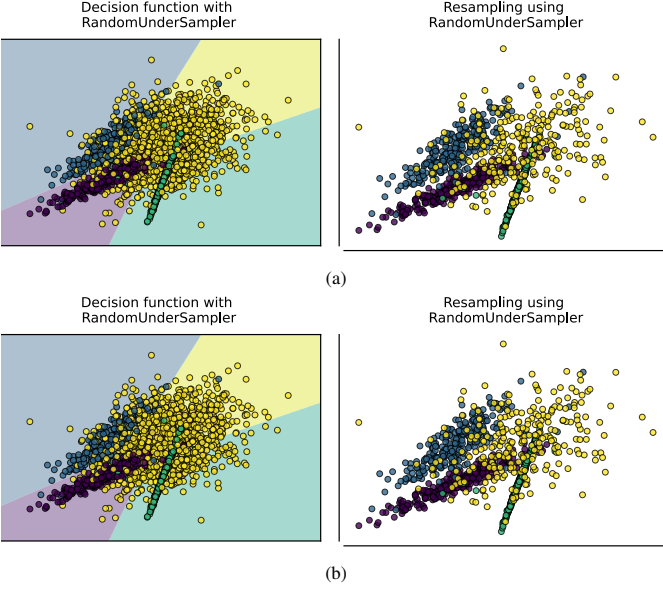


Fig. 11: **Data undersampling before and after processing** by (a) random sampling (b) instance hardness threshold

Table 4: **Impact of transfer learning warm-up.** Here, results are demonstrated for the HierAttn_s model on the IHISIC2019 dataset.

Warm up	Top-1 Accuracy/%
Without	96.28
With	96.70

of 1 and all CTH blocks. Table 5 demonstrates that the stochastic depth effectively enhances the performance of HierAttn_s by 0.65%. Note that even without this stochastic depth, the performance of HierAttn_s delivers similar or better results than SOTA mobile models (Fig. 7).

Table 5: **Impact of stochastic depth.** Here, results are demonstrated for the HierAttn_s model on the IHISIC2019 dataset.

Stochastic depth	Top-1 Accuracy/%
Without	96.05
With	96.70

Skip connection of CTH block. We add a skip connection link in the CTH (convolution-transformer hybrid) block with a stride of 1. Moreover, we also use stochastic depth with those modules with skip connections. Thus, we can not only reuse the lower lever feature but alleviate gradient descent. Table 6 shows a 0.23% improvement in the performance of HierAttn_s with skip connection. Furthermore, MobileViT achieved 0.5% less performance with skip connections on CTH blocks but without stochastic depth (Mehta and Rastegari, 2021). It demonstrates that stochastic depth can reduce the negative influence of adding two distinctive features in the skip connection of the CTH block.

Table 6: **Impact of skip connection.** Here, results are demonstrated for the HierAttn_s model on the IHISIC2019 dataset.

Skip connection	Top-1 Accuracy/%
Without	96.47
With	96.70